Role of the nonmagnetic underlayer in controlling the electronic structure of ferromagnet/nonmagnetic-metal heterostructures

D. Panda,[1] K. K. Behera,[1] S. Madhur,[1] B. Rana,[2] A. Gloskovskii,[3] Y. Otani,[4] A. Barman,[5] and I. Sarkar[1,*]

[1]*Institute of Nano Science and Technology, Sector 81, Sahibzada Ajit Singh Nagar, Punjab 140306, India*

[2]*Institute of Spintronics and Quantum Information, Faculty of Physics, Adam Mickiewicz University in Poznań, Uniwersytetu Poznanskiego 2, 61-614 Poznan, Poland*

[3]*Deutsches Elektronen-Synchrotron DESY, 22607 Hamburg, Germany*

[4]*Center for Emergent Matter Science, RIKEN, Wako, Saitama 351-0198, Japan*

[5]*Department of Condensed Matter and Materials Physics, S. N. Bose National Centre for Basic Sciences, Block JD, Sector III, Salt Lake, Kolkata 700106, India*

(Received 29 April 2024; revised 29 August 2024; accepted 3 September 2024; published 18 September 2024)

Heterostructures comprising of ferromagnet and nonmagnetic metal (NM) interfaces capable of generating spin torque are crucial for next-generation ultrafast magnetic switching devices. Here we present the effect of change of NM underlayer with different spin-orbit coupling (SOC) strength on the spin-dependent electronic structure of quintessential heterostructures of CoFeB/NM. The results reveal deviations from the conventional expectation of the dependence on the strength of SOC of the NM layer. Dichroic photoemission measurements indicate that the spin polarization of the ferromagnetic CoFeB layer is higher with the weaker-SOC Cu underlayer than that with the stronger-SOC Ta, Pt, and W underlayers. The phase space of the unoccupied electronic states near the Fermi level is found more for the W underlayer system than that of the Cu and Ta underlayer systems.

DOI: 10.1103/PhysRevB.110.094424

I. INTRODUCTION

Spin transport across ferromagnet (FM) / non-magnetic metal (NM) is a subject of intense research both for the fundamental understanding of interface phenomenon and from the application point of view in spintronics [1–5]. The various effects of spin transport, like spin pumping (SP), spin orbit torque (SOT), and spin transfer torque (STT) are found to vary based on the nature of the FM/NM layer combination and their spin-orbit coupling (SOC) strength [6–10]. These spin transport effects in FM/NM heterostructures are key factors for ultrafast low-power switching of the magnetic state of the free layer in magnetic tunnel junction (MTJ). The spin transport across the interfaces depend on the spin dependent electronic structure of the FM layer that gets tuned by the presence of NM underlayer. Therefore, it is important to understand the electronic structure evolution of FM/NM as a function of NM layer vis-a-vis observed interfacial spin dynamics and spin transport characteristics. However, an NM layer-dependent electronic structure study in conjunction with spin transfer properties across the FM/NM heterostructure interface has been missing.

CoFeB-based MTJ grown on top of the NM layer is considered as a quintessential technologically relevant heterostructure for spin torque applications [11–14] that will allow the implementation of the next-generation STT and SOT-based magnetic switching devices [15–19]. Therefore, CoFeB/NM provides an ideal model system for understanding FM/NM interface spin property correlation with electronic structure. Ultrafast optical and electrical studies are being extensively pursued to understand and control the spin dynamics, SP, and spin torque efficiencies in CoFeB/NM heterostructures with NM underlayers varied from 4d/5d heavy metals to 3d transition metals [11,20–24]. It is proposed that the observed spin transport properties are related to the increasing strength of the SOC in the NM layer. However, this cannot explain the observed diverse dependence of various interfacial spin-dependent parameters [11,20,24]. For example, the interfacial spin chemical potential shows opposite behavior wherein it is higher for the Cu (3d-element) underlayer system compared to that of W, Pt, Ta (5d-elements) underlayer system [20]. Interestingly, the CoFeB/W system shows much higher spin mixing conductance than the CoFeB/Ta, CoFeB/Pt, and CoFeB/Cu systems. Harmonic Hall measurements show CoFeB/W has more substantial higher-order SOT effects than the CoFeB/Ta [11]. These observations necessitate the study of how the spin-dependent electronic structure of the magnetic layer in the heterostructure gets affected by the presence of an NM underlayer.

Here, we unravel the electronic structure variation of the CoFeB/NM heterostructures with change in the NM layer from Cu (3d-element with weak-SOC) to 5d elements (with strong-SOC) of Ta, Pt, and W using dichroic hard X-ray photoemission spectroscopy (HAXPES) measurements. Intriguingly our results demonstrate that the spin polarization of the magnetic CoFeB layer gets affected by the presence

*Contact author: indranil.sarkar@in

of the NM layer which cannot be directly attributed to a change in the strength of SOC of the NM layer. Furthermore, the change in the phase space of the unoccupied states near the Fermi level in these FM/NM heterostructures is found to be uncorrelated to the SOC of the NM layer. A major problem in obtaining electronic structure information from heterostructures comprising of buried layers is that the conventional photoemission techniques are surface sensitive and have insufficient information depth. The advantage of using HAXPES is that it enables determining the electronic structure measurements of buried layers in a heterostructure due to the enhanced inelastic mean free path of the photo-emitted electrons [25,26]. On the other hand, excitation with circular polarized X-rays leads to spin-selective dichroic photoemission from the 2p-core level of the ferromagnetic layer [27–31].

II. EXPERIMENTAL METHODS

For this study, $Si/SiO_2/NM(10)/Co_{20}Fe_{60}B_{20}(5)/MgO(2)/Al_2O_3(10)$ heterostructures having interfacial roughness of less than 2Å were grown using sputtering technique at a base pressure of 10^{-8} Torr on Si/SiO_2 substrates [20]. The numbers in the parenthesis denote the thickness of layers in nanometers. Cu, Ta, and W were used as different NM underlayers. Al_2O_3 serves as the capping layer that prevents degradation of the underlying heterostructure. The details of growth and physical characterization of the NM/CoFeB/MgO heterostructures have been reported previously [20]. The M-H measurements on these samples have been reported previously and the samples show in-plane easy axis of magnetization with a ratio of about 0.65 for remanent to saturation magnetization [20].

Room temperature HAXPES experiments were conducted at hard X-ray photoelectron spectroscopy beamline at PETRA III (DESY, Hamburg) synchrotron facility [32]. The measurements were carried out using X-ray photons having 6 KeV energy that provided sufficient inelastic mean free path for the photoemitted electrons. This allowed the electronic structure information to be obtained from the buried magnetic layer in the NM/CoFeB heterostructure. The X-ray photons were set at 6 KeV energy using Si(311) reflection of a double crystal monochromator yielding high degree of energy resolution. The X-ray photons were incident on the sample at a grazing incidence angle of 5° and measurements were made at normal emission using a SPECS PHOIBOS 225 HV hemispherical electron energy analyzer. For dichroic HAXPES, circularly polarized X-ray photons were used and the samples were *in-situ* remanently in-plane magnetized inside the UHV chamber. The circular polarization was obtained by an in-vacuum diamond single crystal based phase retarder. The photon helicity was switched between left (σ^-) and right (σ^+) circular polarization for dichroic measurements.

In a photoemission experiment a core-electron is photoemitted leaving behind a core-hole. In a magnetic material the spin of this core-hole interacts with the spin-polarized valence electrons through an effective spin/magnetic field that depends on the strength of spin polarization of the valence state near Fermi level [33,34]. This can cause splitting of core-hole state whose strength shall depend on the spin polarization of the valence state. This splitting leads to dichroism in photoemission signal for opposite polarization of photoexcitation. Additionally, spin of core-hole can interact with orbital moment of valence state through spin-orbit interaction that can lead to spin-orbit split core-hole bands [33]. In case of Fe-2p and Co-2p photoemission, spin-orbit split peaks are well separated allowing for a clear study of spin-polarized valence electron mediated splitting of 2p-core-levels [27,28,33]. Therefore, through dichroic photoemission study on 2p-levels it is possible to study the behavior of spin polarization in magnetic materials [33,34].

III. RESULTS AND DISCUSSION

Figure 1 shows dichroic photoemission spectra of Fe-2p core level recorded for CoFeB/NM (NM = Cu, W, Ta, Pt) heterostructures. The spectra show the typical spin-orbit split peaks corresponding to the Fe-$2p_{3/2}$ and Fe-$2p_{1/2}$ states separated by about 13eV [35]. The σ^+ and σ^- spectra show [Figs. 1(a)–1(c)] clear dichroism. This difference can be understood as a combination of the change in photon-electron coupling strength for the different helicity of polarized light and the lifting of spin degeneracy of core level due to the exchange interaction of core-hole spin with the spin polarization of the valence band [27–31]. The exchange interaction can be thought of as an effective magnetic field (H_s) that lifts the degeneracy of the spin-orbit split Fe $2p_{3/2}$ and Fe $2p_{1/2}$ core levels into different m_j states where former splits in m_j = -3/2, -1/2, 1/2, 3/2 levels and the latter splits in m_j = 1/2, -1/2 levels [29]. In the strong spin-orbit coupling limit the energy shifts of the $|j, m_j\rangle$ sublevels due to H_s, is given by [29]

$$E_{j,m_j} = H_s m_j \frac{j(j+1) + s(s+1) - l(l+1)}{2j(j+1)}. \quad (1)$$

Therefore, for Fe-$2p_{3/2}$ (j = 3/2) peak, the m_j = -3/2 and +3/2 are respectively the lowest and highest binding energy state. While m_j = 1/2 and -1/2 are respectively the lowest and highest binding energy state for Fe $2p_{1/2}$ peak. The maximum coupling between photon and electron occurs when the angular momentum (J_z) of the former aligns with total angular momentum of the latter [33,35]. This leads to reduced emission from m_j = -3/2 and -1/2 states for σ^+ (J_z = +1) excitation. While for σ^- (J_z = -1) excitation emission is reduced from m_j = 3/2 and 1/2 states.

The dichroic asymmetry of Fe-2p spectra was calculated [Figs. 2(a)–2(d)] by normalizing the difference of σ^+ and σ^- spectra with the sum of maxima of the two spectra. Intriguingly, there is a strong variation in the asymmetry of Fe-2p photoemission (Fig. 2) for different NM underlayer systems, although the signal arises from the magnetic CoFeB layer. The highest asymmetry is observed [Fig. 2(d)] in Cu underlayer heterostructure with a maximum value reaching up to 0.21. On the other hand, the dichroic asymmetry of the heavy metal underlayer systems based on Ta, Pt, and W show similar asymmetry behavior with a maximum value reaching around 0.9 which is less than half of that observed in the CoFeB/Cu heterostructure. These observations are further corroborated by similar NM layer dependence of dichroic photoemission [Figs. 3(a)–3(d)] and dichroic asymmetry [Figs. 4(a)–4(d)]

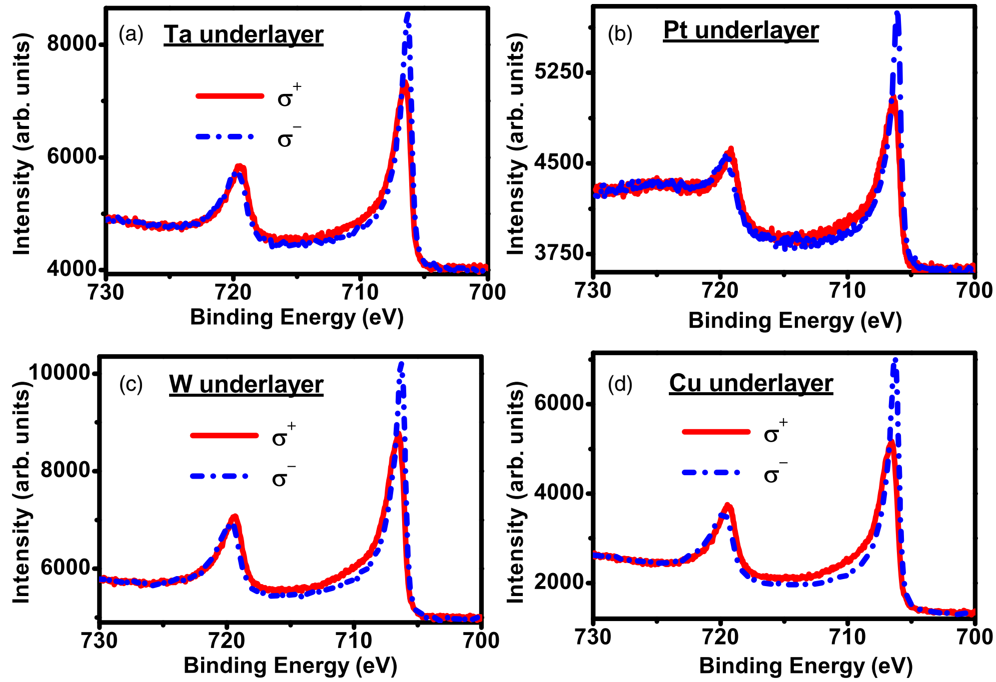

FIG. 1. Dichroic Fe-2p HAXPES intensity ($I^{\sigma^{\pm}}$) versus binding energy data recorded using right σ^+ and left σ^- polarized X-ray photons recorded on (a) CoFeB/Ta, (b) CoFeB/Pt, (c) CoFeB/W, and (d) CoFeB/Cu heterostructures.

of Co-2p core level for CoFeB/NM heterostructure. As the strength of dichroic asymmetry depends on the strength of interaction between the core-hole and the spin polarization of the valence band [27,29], the higher asymmetry is indicative of higher spin polarization. Therefore, the dichroic photoemission measurements indicate that CoFeB/Cu system has higher spin polarization than the heterostructures of CoFeB/Ta, CoFeB/Pt, and CoFeB/W, where the latter three have comparable values. This is interesting as Ta, Pt, and W (5d elements) have higher intrinsic spin-orbit coupling (SOC)

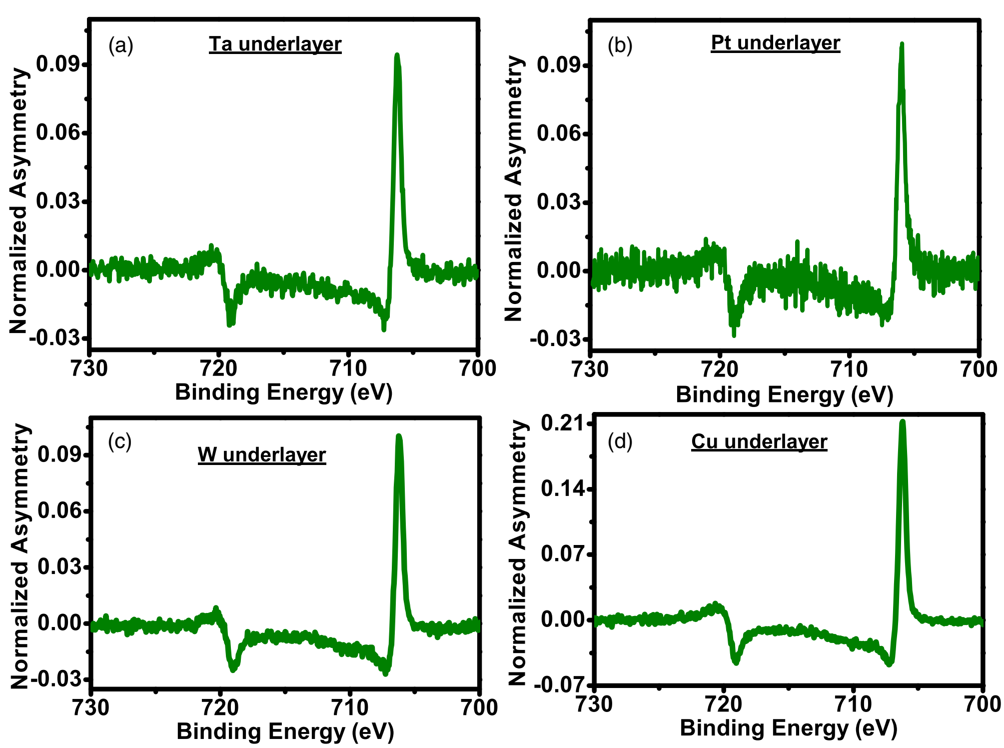

FIG. 2. Calculated Fe-2p dichroic asymmetry $((I^{\sigma-} - I^{\sigma+})/(I^{\sigma+}_{\max} + I^{\sigma-}_{\max}))$ for (a) CoFeB/Ta, (b) CoFeB/Pt, (c) CoFeB/W, and (d) CoFeB/Cu heterostructures.

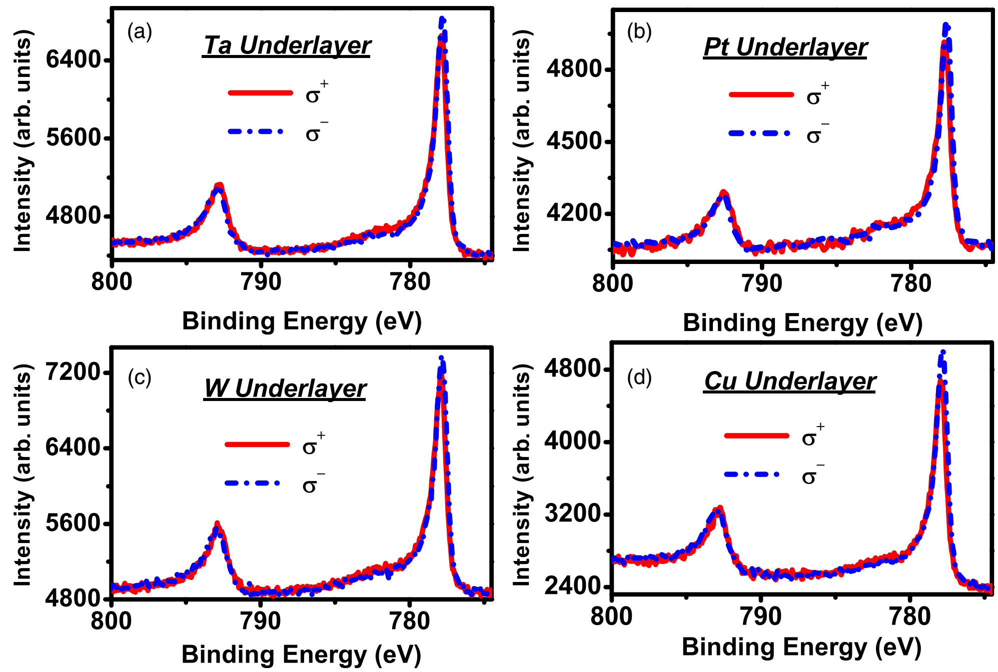

FIG. 3. Dichroic Co-2p HAXPES intensity ($I^{\sigma\pm}$) versus binding energy data recorded using right σ^+ and left σ^- polarized X-ray photons recorded on (a) CoFeB/Ta, (b) CoFeB/Pt, (c) CoFeB/W, and (d) CoFeB/Cu heterostructures.

than Cu (3d element) which is opposite to the observed indication of spin-polarization dependence on the NM layer in the CoFeB/NM heterostructures. Therefore, these results show that the spin polarization of the magnetic layer gets affected in proximity to the nonmagnetic layer and this change does not necessarily vary with the strength of the SOC of the NM layer.

The NM layer dependence of spin polarization of FM/NM heterostructure has an important consequence on the spin accumulation at the interface and consequently on the interfacial spin chemical potential. This can be understood based on Mott's two-current model that assumes conductivity of the majority and minority spin channels as independent and different [36]. A consequence of which in FM/NM

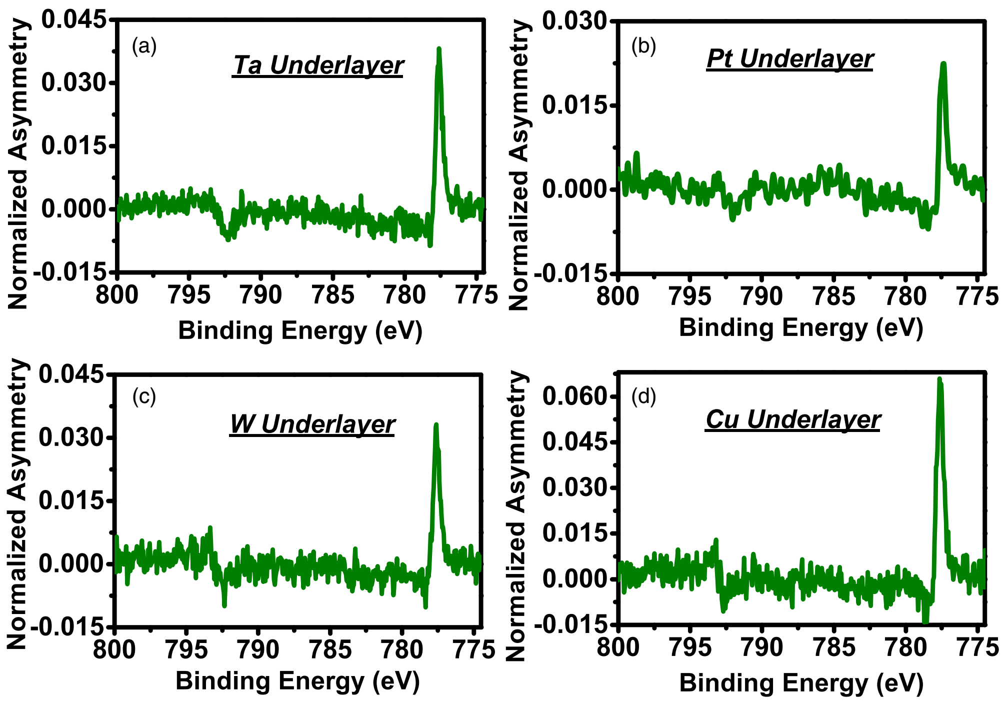

FIG. 4. Calculated Co-2p dichroic asymmetry $((I^{\sigma-} - I^{\sigma+})/(I^{\sigma+}_{\max} + I^{\sigma-}_{\max}))$ for (a) CoFeB/Ta, (b) CoFeB/Pt, (c) CoFeB/W, and (d) CoFeB/Cu heterostructures.

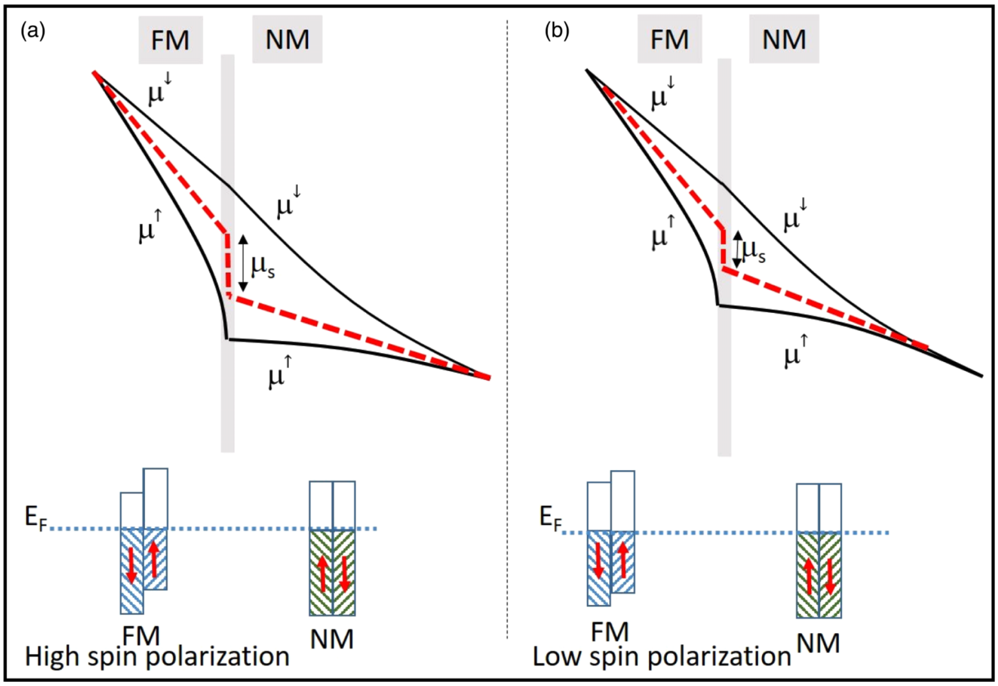

FIG. 5. Representative picture of spin dependent chemical potential (μ) for ferromagnet/non-magnetic metal interface in presence of current flow from (a) a high-spin polarized FM layer to NM layer and (b) low-spin polarized FM Layer to NM layer. Representative density of states for high- and low-spin polarization at the Fermi level for the FM layer is shown at the lower panel.

heterostructure is lower resistance to minority spin flow in the NM layer causing depletion of minority spins at the FM/NM interface [37]. This leads to accumulation of majority spins at the interface [36,38]. On the other hand, the spin accumulation determines the strength of interfacial spin chemical potential (μ_s) [37]. Therefore, higher spin accumulation should lead to higher interfacial spin chemical potential (μ_s) in FM/NM heterostructure having higher spin polarization (Fig. 5 shows a representative picture). The larger spin polarization of the FM layer implies more occupied majority spin states while less occupied minority spin states at the Fermi level (bottom panel Fig. 5). Therefore, our observation of higher spin polarization for CoFeB/Cu system may lead to higher spin accumulation in CoFeB/Cu compared to that of CoFeB/NM (NM = W, Pt, and Ta) heterostructures. Such an interfacial spin accumulation can exert spin torque on the neighboring FM layer [39]. This variation in spin accumulation in the CoFeB/NM heterostructure is corroborated by previously reported μ_s values measured on these samples using magnetization dynamics measurements based on TR-MOKE technique [20]. TR-MOKE measurements have yielded a μ_s value of ≈1.45 eV in CoFeB/Cu that is an order of magnitude higher compared to that in CoFeB/W, CoFeB/Pt, and CoFeB/Ta heterostructures [20]. Table I shows a comparison of values of μ_s obtained from TR-MOKE measurements [20] and normalized dichroic asymmetry for Fe-2p.

Figure 6 shows the background subtracted Fe-2$p_{3/2}$ spectra recorded using X-ray photons without circular polarization. The data shows the typical asymmetric shape for metallic systems with a tailing due to spectral weight shift towards the higher binding energy side [40,41]. The tailing is related to the energy loss of the photo-emitted electron due to transfer of energy leading to many small excitations (inset Fig. 6) of the valence edge electrons to the available unoccupied states above the Fermi level [40,41]. Therefore, the degree of tailing indicates the availability of unoccupied states for the electrons. The data show that the CoFeB/W has more significant spectral weight shift towards higher binding energy than in CoFeB/Ta, CoFeB/Pt, and CoFeB/Cu. The latter three have similar behavior. This is interesting as it suggests that a larger phase space of unoccupied states near the Fermi level is available for the electrons in the case of CoFeB/W. This may be related to higher density of unoccupied states near the Fermi level for W, as found in electronic structure calculations [42]. Though the SOC strength of W, Pt, and Ta are similar while that of Cu is much weaker, the unoccupied states for Fermi-level electrons is more in the W underlayer system than that in the Ta, Pt, and Cu underlayer systems. This indicates that the degree of available uncoupled states near the Fermi level in FM/NM heterostructure though is affected by the underlayer but it does not directly correlate with the SOC strengths of the NM layer. Fermi-level electrons are the ones responsible for carrying spin currents, therefore, this NM underlayer-dependent change in unoccupied states near the

TABLE I. The value of μ_s as obtained in a previous TR-MOKE study [20] and maximum normalized dichroic asymmetry for Fe-2p for different NM underlayer systems.

NM underlayer	μ_s (eV)	Normalized dichroic asymmetry
Cu	≈1.46 [20]	0.21 (±0.005)
Pt	≈0.12 [20]	0.1 (±0.005)
Ta	≈0.26 [20]	0.095 (±0.005)
W	≈0.1 [20]	0.097 (±0.005)

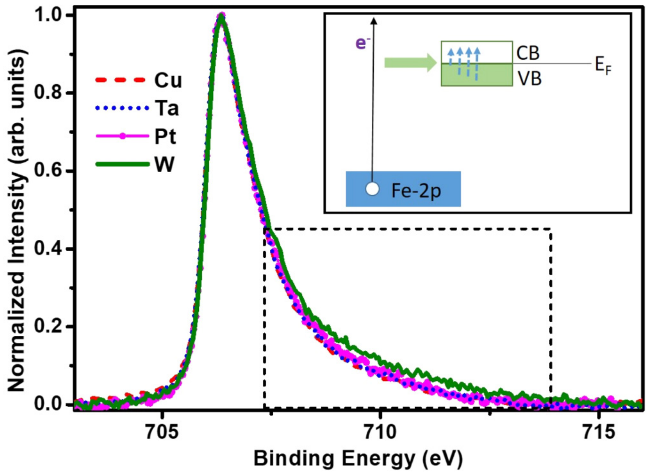

FIG. 6. Background subtracted normalized Fe-2$p_{3/2}$ spectra recorded for CoFeB/ NM heterostructure for W,Ta, Pt, and Cu underlayers using linearly polarized X-ray photons. Normalization is done with respect to the peak intensity of the respective spectra. Shirley background has been subtracted from the data (*cf* Supplemental Material [46]). The square box indicates the region of tailing where clear differences are observed for the W underlayer system compared to that of Ta, Pt, and Cu systems. The inset shows a representative picture of loss of energy of the photo-emitted Fe 2p core level electron in creating small energy excitations (shown by dotted arrows across the Fermi level) from valence band (VB) to the conduction band (CB).

Fermi level should affect the spin transport properties such as magnetic Gilbert damping and spin-mixing conductance across the interface of FM/NM heterostructure.

Magnetic Gilbert damping is understood by generalized torque correlation models arising due to spin-orbit torque induced scattering between electronic states, wherein the scattering term is weighted by the spectral overlap and the density of states near the Fermi level [43,44]. For such scattering to occur unoccupied states are required. Therefore, any change in availability of unoccupied states shall affect the rate of electronic scattering and consequently the magnetic damping. Thus, the observed increase in unoccupied states for scattering in CoFeB/W should lead to an increase in magnetic damping. This explains and reconciles with the earlier TR-MOKE measurements [20] where a much higher value of magnetic damping of around 0.024 is found in the case of CoFeB/W compared to a lower value of less than 0.015 for heterostructures with Ta, Cu, and Pt underlayers [20]. Furthermore, the spin-mixing conductance determines the interface transparency for spin current across the FM/NM layer [8]. The higher the spin mixing conductance, the better is the transmission of spin current ac ross the interface and consequently the better are the spin torque effects [8]. On the other hand the spin mixing conductance is proportional to the reflection matrix of scattering states at the Fermi energy of the normal and ferromagnetic metal [45]. Therefore, the availability of more unoccupied states near the Fermi level for CoFeB/W heterostructure should provide more scattering states that should lead to higher spin-mixing conductance. This is corroborated by the previous measurements of three times higher spin-mixing conductance in CoFeB/W compared to that of CoFeB/Ta and CoFeB/Cu [20].

IV. CONCLUSION

To conclude, through spin selective dichroic hard X-ray photoemission studies on FM/NM spin torque heterostructure, we have presented the effect of the nonmagnetic layer with varying SOC strength on the spin-polarized electronic structure of the ferromagnetic layer and on the availability of the unoccupied electronic states near the Fermi level. A comprehensive study for different NM underlayer having weak to strong SOC strength has been carried out on the technologically important class of CoFeB/NM system that also serves as a quintessential model system for spin transfer effects at FM/NM interfaces. The results show that the effect of the NM layer on the electronic structure that determines the interfacial spin transfer properties cannot be accounted for within the conventional consideration based on the strength of SOC of the NM layer. These results present critical insights into the electronic structure of spin torque generating FM/NM heterostructures that will open new avenues both for fundamental understanding and for designing and controlling spin transfer properties across FM/NM heterostructures.

ACKNOWLEDGMENTS

I.S. gratefully acknowledges funding from Nano Mission, Department of Science and Technology (DST), Govt. of India under Grant No. DST/NM/TUE/QM-3/2019-1G-INST. I.S. acknowledges financial support by DST-India provided within the framework of India@Desy collaboration. BR acknowledges NCN SONATA-16 project with Grant No. 2020/39/D/ST3/02378.

[1] M. A. W. Schoen, D. Thonig, M. L. Schneider, T. J. Silva, H. T. Nembach, O. Eriksson, O. Karis, and J. M. Shaw, Ultra-low magnetic damping of a metallic ferromagnet, Nat. Phys. **12**, 839 (2016).

[2] W. Wang, T. Wang, V. P. Amin, Y. Wang, A. Radhakrishnan, A. Davidson, S. R. Allen, T. J. Silva, He. Ohldag, D. Balzar, B. L. Zink, P. M. Haney, J. Q. Xiao, D. G. Cahill, V. O. Lorenz, and X. Fan, Anomalous spin–orbit torques in magnetic single-layer films, Nat. Nanotechnol. **14**, 819 (2019).

[3] Y. Li, D. Zheng, B. Fang, C. Liu, C. Zhang, A. Chen, Y. Ma, K. Shen, H. Liu, A. Manchon, X. Zhang, Unconventional spin pumping and magnetic damping in an insulating compensated ferrimagnet, Adv. Mater. **34**, 2200019 (2022).

[4] A. Brataas, Quantum scattering theory of spin transfer torque, spin pumping, and fluctuations, Phys. Rev. B **106**, 064402 (2022).

[5] A. Hoffmann, Spin pumping gathers speed, Science **368**, 135 (2020).

[6] D. Zhu, T. Zhang, X. Fu, R. Hao, A. Hamzic, H. Yang, X. Zhang, H. Zhang, A. Du, D. Xiong, K. Shi, S. Yan, S. Zhang, A. Fert, and W. Zhao, Sign change of spin-orbit torque in Pt/NiO/CoFeB structures, Phys. Rev. Lett. **128**, 217702 (2022).

[7] D. Jhajhria, N. Behera, D. K. Pandya, and S. Chaudhary, Dependence of spin pumping in W/CoFeB heterostructures on the structural phase of tungsten, Phys. Rev. B **99**, 014430 (2019).

[8] W. Zhang, W. Han, X. Jiang, S. H. Yang, and S. S. P. Parkin, Role of transparency of platinum–ferromagnet interfaces in determining the intrinsic magnitude of the spin Hall effect, Nat. Phys. **11**, 496 (2015).

[9] J. Ryu, S. Lee, K. J. Lee, B. G. Park, Current-induced spin–orbit torques for spintronic applications, Adv. Mater. **32**, 1907148 (2020).

[10] L. Zhu, D. C. Ralph, and R. A. Buhrman, Spin-orbit torques in heavy-metal–ferromagnet bilayers with varying strengths of interfacial spin-orbit coupling, Phys. Rev. Lett. **122**, 077201 (2019).

[11] E. S. Park, D. K. Lee, F. Xue, B. C. Min, H. C. Koo, P. M. Haney, K. W. Kim, and K. J. Lee, Strong higher-order angular dependence of spin-orbit torque in W/CoFeB bilayer, Phys. Rev. B **107**, 064411 (2023).

[12] J. Wei, C. He, X. Wang, H. Xu, Y. Liu, Y. Guang, C. Wan, J. Feng, G. Yu, and X. Han, Characterization of spin-orbit torque efficiency in magnetic heterostructures with perpendicular magnetic anisotropy via spin-torque ferromagnetic resonance, Phys. Rev. Appl. **13**, 034041 (2020).

[13] M. Shinozaki, J. Igarashi, S. Iwakiri, T. Kitada, K. Hayakawa, B. Jinnai, T. Otsuka, S. Fukami, K. Kobayashi, and H. Ohno, Nonlinear conductance in nanoscale CoFeB/MgO magnetic tunnel junctions with perpendicular easy axis, Phys. Rev. B **107**, 094436 (2023).

[14] Z. Wang, M. Saito, K. P. McKenna, S. Fukami, H. Sato, S. Ikeda, H. Ohno, and Y. Ikuhara, Atomic-scale structure and local chemistry of CoFeB–MgO magnetic tunnel junctions, Nano Lett. **16**, 1530 (2016).

[15] K. Jhuria, J. Hohlfeld, A. Pattabi, E. Martin, A. Ygnacio, A. Córdova, X. Shi, R. L. Conte, S. P. Watelot, J. C. R. Sanchez, G. Malinowski, S. Mangin, A. Lemaître, M. Hehn, J. Bokor, R. B. Wilson, and J. Gorchon, Spin–orbit torque switching of a ferromagnet with picosecond electrical pulses, Nat. Electron. **3**, 680 (2020).

[16] A. Meo, S. Sampan-a-pai, P. B. Visscher, R. Chepulskyy, D. Apalkov, J. Chureemart, P. Chureemart, R. W. Chantrell, and R. F. L. Evans, Spin transfer torque switching dynamics in CoFeB/MgO magnetic tunnel junctions, Phys. Rev. B **103**, 054426 (2021).

[17] K. Watanabe, B. Jinnai, S. Fukami, H. Sato, and H. Ohno, Shape anisotropy revisited in single-digit nanometer magnetic tunnel junctions, Nat. Commun. **9**, 663 (2018).

[18] M. Wang, W. Cai, K. Cao, J. Zhou, J. Wrona, S. Peng, H. Yang, J. Wei, W. Kang, Y. Zhang, J. Langer, B. Ocker, A. Fert, and W. Zhao, Current-induced magnetization switching in atom-thick tungsten engineered perpendicular magnetic tunnel junctions with large tunnel magnetoresistance Nat. Commun. **9**, 671 (2018).

[19] H. Fulara, M. Zahedinejad, R. Khymyn, M. Dvornik, S. Fukami, S. Kanai, H. Ohno, and J. Akerman, Giant voltage-controlled modulation of spin Hall nano-oscillator damping, Nat. Commun. **11**, 4006 (2020).

[20] S. N. Panda, B. Rana, Y. Otani, and A. Barman, Role of spin–orbit coupling on ultrafast spin dynamics in nonmagnet/ferromagnet heterostructures, Adv. Quantum Technol. **5**, 2200016 (2022).

[21] C. von KorffSchmising, S. Jana, K. Yao, M. Hennecke, P. Scheid, S. Sharma, M. Viret, J. Y. Chauleau, D. Schick, and S. Eisebitt, Ultrafast behavior of induced and intrinsic magnetic moments in CoFeB/Pt bilayers probed by element-specific measurements in the extreme ultraviolet spectral range, Phys. Rev. Res. **5**, 013147 (2023).

[22] X. Sui, C. Wang, J. Kim, J. Wang, S. H. Rhim, W. Duan, and N. Kioussis, Giant enhancement of the intrinsic spin Hall conductivity in β-tungsten via substitutional doping, Phys. Rev. B **96**, 241105(R) (2017).

[23] S. Iihama, S. Mizukami, H. Naganuma, M. Oogane, Y. Ando, and T. Miyazaki, Gilbert damping constants of Ta/CoFeB/MgO(Ta) thin films measured by optical detection of precessional magnetization dynamics, Phys. Rev. B **89**, 174416 (2014).

[24] A. Conca, B. Heinz, M. R. Schweizer, S. Keller, E. T. Papaioannou, and B. Hillebrands, Lack of correlation between the spin-mixing conductance and the inverse spin Hall effect generated voltages in CoFeB/Pt and CoFeB/Ta bilayers, Phys. Rev. B **95**, 174426 (2017).

[25] G. H. Fecher, B. Balke, A. Gloskowskii, S. Ouardi, C. Felser, T. Ishikawa, M. Yamamoto, Y. Yamashita, H. Yoshikawa, S. Ueda, and K. Kobayashi, Detection of the valence band in buried tunnel junctions by means of photoemission spectroscopy, Appl. Phys. Lett. **92**, 193513 (2008).

[26] S. Ueda, Application of hard X-ray photoelectron spectroscopy to electronic structure measurements for various functional materials, J. Electron Spectrosc. Relat. Phenom. **190**, 235 (2013).

[27] L. Baumgarten, C. M. Schneider, H. Petersen, F. Schafers, and J. Kirschner, Magnetic x-ray dichroism in core-level photoemission from ferromagnets, Phys. Rev. Lett. **65**, 492 (1990).

[28] H. Ebert, L. Baumgarten, C. M. Schneider, and J. Kirschner, Polarization dependence of the 2*p*-core-level photoemission spectra of Fe, Phys. Rev. B **44**, 4406 (1991).

[29] G. van der Laan, Zen and the art of dichroic photoemission, J. Electron Spectrosc. Relat. Phenom. **200**, 143 (2015).

[30] W. Kuch and C. M. Schneider, Magnetic dichroism in valence band photoemission, Rep. Prog. Phys. **64**, 147 (2001).

[31] E. Arenholz, E. Navas, K. Starke, L. Baumgarten, and G. Kaindl, Magnetic circular dichroism in core-level photoemission from Gd, Tb, and Dy in ferromagnetic materials, Phys. Rev. B **51**, 8211 (1995).

[32] C. Schlueter, A. Gloskovskii, K. Ederer, I. Schostak, S. Piec, I. Sarkar, Y. Matveyev, P. Lömker, M. Sing, R. Claessen, C. Wiemann, C. M. Schneider, K. Medjanik, G. Schönhense, P. Amann, A. Nilsson, and W. Drube, The new dedicated HAXPES beamline P22 at PETRAIII, AIP Conf. Proc. **2054**, 040010 (2019).

[33] G. Van der Laan, Angular-resolved linear and circular dichroism in core-level photoemission of metallic systems, Phys. Rev. B **51** 240 (1995).

[34] B. T. Thole and G. van der Laan, Spin polarization and magnetic dichroism in photoemission from core and valence states in localized magnetic systems. III. Angular distributions, Phys. Rev. B **49**, 9613 (1994).

[35] F. U. Hillebrecht, Ch. Roth, H. B. Rose, W. G. Park, E. Kisker, and N. A. Cherepkov, Magnetic linear dichroism in spin-resolved Fe 2*p* photoemission, Phys. Rev. B **53**, 12182 (1996).
[36] P. C. van Son, H. van Kempen, and P. Wyder, Boundary resistance of the ferromagnetic-nonferromagnetic metal interface, Phys. Rev. Lett. **58**, 2271 (1987).
[37] W. Zhang, Q. Liu, Z. Yuan, K. Xia, W. He, Q. F. Zhan, X. Q. Zhang, and Z. H. Cheng, Enhancement of ultrafast demagnetization rate and Gilbert damping driven by femtosecond laser-induced spin currents in bilayers, Phys. Rev. B **100**, 104412 (2019).
[38] R. Kukreja, S. Bonetti, Z. Chen, D. Backes, Y. Acremann, J. A. Katine, A. D. Kent, H. A. Durr, H. Ohldag, and J. Stohr, X-ray detection of transient magnetic moments induced by a spin current in Cu, Phys. Rev. Lett. **115**, 096601 (2015).
[39] A. Manchon and S. Zhang, Theory of nonequilibrium intrinsic spin torque in a single nanomagnet, Phys. Rev. B **78**, 212405 (2008).
[40] J. C. W. Folmer, D. K. G. de Boer, XPS core level line shapes in metallic compounds: A probe for the nature of the electrons at the Fermi level, Solid State Commun. **38**, 1135 (1981).
[41] F. de Groot and A. Kotani, *Core Level Spectroscopy of Solids* (CRC Press, Taylor and Francis Group, Boca Raton, FL, 2008).
[42] Z. Lin, L. V. Zhigilei, and V. Celli, Electron-phonon coupling and electron heat capacity of metals under conditions of strong electron-phonon nonequilibrium, Phys. Rev. B **77**, 075133 (2008).
[43] K. Gilmore, Y. U. Idzerda, and M. D. Stiles, Identification of the dominant precession-damping mechanism in Fe, Co, and Ni by first-principles calculations, Phys. Rev. Lett. **99**, 027204 (2007).
[44] H. Ebert, S. Mankovsky, D. Kodderitzsch, and P. J. Kelly, *Ab initio* calculation of the Gilbert damping parameter via the linear response formalism, Phys. Rev. Lett. **107**, 066603 (2011).
[45] M. Zwierzycki, Y. Tserkovnyak, Pa. J. Kelly, A. Brataas, and G. E. W. Bauer, First-principles study of magnetization relaxation enhancement and spin transfer in thin magnetic films, Phys. Rev. B **71**, 064420 (2005).
[46] See Supplemental Material at http://link.aps.org/supplemental/10.1103/PhysRevB.110.094424 for background fitted data of Fe-2$p_{3/2}$ spectra for CoFeB/NM heterostructure recorded using linearly polarized X-rays.